## PAPER

# Light-emitting Ga-oxide nanocrystals in glass: a new paradigm for low-cost and robust UV-to-visible solar-blind converters and UV emitters†

Vladimir N. Sigaev,[a] Nikita V. Golubev,[a] Elena S. Ignat'eva,[a] Alberto Paleari*[ab] and Roberto Lorenzi[b]

Wide-bandgap nanocrystals are an inexhaustible source of tuneable functions potentially addressing most of the demand for new light emitting systems. However, the implementation of nanocrystal properties in real devices is not straightforward if a robust and stable optical component is required as a final result. The achievement of efficient light emission from dense dispersions of Ga-oxide nanocrystals in UV-grade glass can be a breakthrough in this regard. Such a result would permit the fabrication of low cost UV-to-visible converters for monitoring UV-emitting events on a large-scale – from invisible hydrogen flames to corona dispersions. From this perspective, $\gamma\text{-}Ga_2O_3$ nanocrystals are developed by phase separation in Ga-alkali-germanosilicate glasses, obtaining optical materials based on a UV transparent matrix. Band-to-band UV-excitation of light emission from donor−acceptor pair (DAP) recombination is investigated for the first time in embedded $\gamma\text{-}Ga_2O_3$. The analysis of the decay kinetics gives unprecedented evidence that nanosized confinement of DAP recombination can force a nanophase to the efficient response of exactly balanced DAPs. The results, including a proof of concept of UV-to-visible viewer, definitely demonstrate the feasibility of workable glass-based fully inorganic nanostructured materials with emission properties borrowed from $Ga_2O_3$ single-crystals and tailored by the nanocrystal size.

## Introduction

Gallium oxide nanophases are investigated in different fields in view of exploiting several intriguing properties strictly related to the possibility of reproducing at a nanoscale the response of a wide bandgap system. These properties include intense UV-excited light emission,[1] relatively efficient charge transport mechanisms,[2] and the possible occurrence of insulator-to-metal transition.[3] Based on these properties, several applications of Ga oxide nanophases have been envisaged in recent years in the field of light-emitting materials,[4,5] in optoelectronics,[6,7] and in the fields of sensors and communication systems.[8,9] Much of the interest is in the efficient light emission, whose broad excitation at wavelengths shorter than 280 nm is strictly related to the direct allowed optical gap of the material. The main luminescence band is centered in the blue region at around 460 nm and is connected to radiative recombination at donor and acceptor pairs (DAPs). DAPs in Ga oxides consist of an oxygen vacancy $V_O^{\cdot}$, acting as a donor, and an association of oxygen and gallium vacancies in $(V_O, V_{Ga})'$ sites, behaving as acceptors.[10] Additional emissions in the green and UV regions are sometimes observed, at 550 nm, probably from electron–hole recombination between $V_O^{\cdot}$ and $V_{Ga}$ sites, and in the 340–390 nm range. The UV emission arises from exciton-like decay mediated by sub-band gap levels, mainly observed in doped materials but also in pure single crystals.[7,10–14]

Since UV-excited light emission is accompanied by good transmittance and no excitation channel in the whole visible and near-UV spectrum, $Ga_2O_3$-based materials can be considered particularly suitable systems, in principle, for the fabrication of simple and robust fully inorganic UV-to-visible converters. Such optical components could be coupled to silicon-based commercial detectors for the imaging of UV events, without any signal intensifier, which makes the visible view problematic under daylight conditions for saturation, unless some complex double detection system is employed. The excitation threshold at 280 nm coincides in fact with the long-wavelength limit of the UV-C spectral region above which the solar spectrum at the Earth surface does not give any detrimental background to the detection of UV-emitting events. For this reason, important results have recently been obtained in

[a]P.D. Sarkisov International Laboratory of Glass-based Functional Materials, Mendeleev University of Chemical Technology of Russia, Miusskaya Square 9, 125190 Moscow, Russia

[b]Department of Materials Science, University of Milano-Bicocca, Via R. Cozzi 55, I-20125 Milano, Italy. E-mail: alberto.paleari@unimib.it; Fax: +39 02 64485400; Tel: +39 02 64485164

† Electronic supplementary information (ESI) available. See DOI: 10.1039/c3nr05210a

the field of optoelectronic solar-blind 'active' transducers by means of Ga-oxide nanowire assemblies.[8] Instead, the production of crystalline Ga-oxide as optical quality macroscopic components for 'passive' UV-to-visible windows is too expensive to be competitive with devices employing UV-sensitive or intensified detectors, even though quite complex and expensive. At present, the lack of low-cost alternative solutions for simultaneous UV and visible imaging prevents us from monitoring on a large-scale a wide variety of UV-emitting invisible events, which can affect human safety conditions in working places, energy-saving, and electric power distribution reliability, such as hydrogen flames, electric sparks, and corona dispersions in high-voltage lines.

In this view, we envisaged that a novel strategy toward a potential breakthrough could be proposed, thanks to a method for obtaining Ga-containing optical quality nanostructured glass through low-cost glass melting techniques and controlled growth of $\gamma$-$Ga_2O_3$ nanocrystals (NCs).[15–17] At present, however, data on light emission properties of nanosized Ga oxides are only available for nanopowders and nanowires, or NCs in colloidal solutions.[14,18–25] A large fraction of those results regard the $\beta$-$Ga_2O_3$ phase,[4,6,7,10–14,22] whereas only a few studies concern the metastable polymorph $\gamma$-$Ga_2O_3$.[5,18–21,24,25] No work to our knowledge has ever tackled the task of investigating the intrinsic light emission of $\gamma$-$Ga_2O_3$ NCs dispersed in glass matrices. In such systems, the stabilization and possible passivation of the nanophase inside the host, as well as the interaction with the surrounding glass, can in principle give rise to results different from those obtained in free-standing nanosystems.[26]

Here we show for the first time that $\gamma$-$Ga_2O_3$ NCs behave as efficient light emitting nanosystems in optical quality glass obtained from Ga-containing alkali-germanosilicate glass. We present detailed data on the excitation–emission pattern and the optical absorption edge. We also analyze the temperature dependence of the emitted intensity, the decay kinetics, and the effects induced by changing the DAP population upon heterovalent doping. As a result, we demonstrate the feasibility of optical quality nanostructured glass, which preserves the intrinsic light-emission properties of Ga-oxide nanophases. Importantly, we also show how the population of intrinsic acceptor and donor sites can be controlled by selective doping. In this way, UV and blue emissions can be optimized for different purposes, including solar-blind UV-to-blue converters[8,9] and UV-emitting devices.[27]

## Materials and procedure

Glass with nominal molar composition 7.5$Li_2O$–2.5$Na_2O$–20$Ga_2O_3$–35$SiO_2$–35$GeO_2$ was prepared by a conventional melt-quenching method, using, as raw materials, amorphous $SiO_2$ (special purity grade), $GeO_2$ (special purity), $Li_2CO_3$ (reagent grade), $Na_2CO_3$ (reagent grade), and $Ga_2O_3$ (reagent grade). Ni-doped samples were prepared by adding 0.05, 0.1, and 1 mol % NiO (reagent grade). A Ga-free reference sample with a molar composition of 9.4$Li_2O$–3.0$Na_2O$–43.8$SiO_2$–43.8$GeO_2$ was also prepared, following the same procedure and keeping unchanged the proportions of the other oxide components. In all cases, the amount of reagent in each batch was calculated in order to prepare up to 120 g of final product. The starting materials were weighed using an analytical balance with an accuracy of 0.001 g and carefully mixed in an agate mortar. Glass was then prepared in a 40 ml crucible in air at 1480 °C for 40 min. The as-quenched bulk samples were heat treated at a temperature of nanocrystallization of about 690 °C, for 15 min, except in specific cases, aimed at observing the effects of prolonged treatment (2.5 hours). Heat treatment was performed in air by putting the glass samples into the muffle furnace with an accuracy at the heat treatment temperature of ±2 K. Samples were then polished for optical measurements.

Transmission electron microscopy (TEM) images, high resolution TEM (HRTEM) analysis, and electron diffraction patterns were obtained using a field emission gun transmission electron microscope FEI TECNAI G2 F20, with an accelerating voltage of 200 kV and equipped with an S-Twin lens that gives a point resolution of 0.24 nm. The imaging system is composed of one TV rate 626 Gatan and one slow scan 794 Gatan CCD camera. Samples were prepared as a finely ground powder and deposited on a gold microscopy grid. No effect of electron irradiation on the nanostructured materials was observed during low resolution measurements. Differential scanning calorimetry (DSC) measurements were performed by means of a NETZSCH DSC 449F3 high-temperature thermoanalyzer in platinum crucibles, at a heating rate of 10 K min$^{-1}$ in Ar, on bulk samples of 10–15 mg. X-ray diffraction patterns of the powdered samples were recorded on a BRUKER D2 PHASER diffractometer (CuK$\alpha$ radiation, Ni filter). Particular attention has been paid to specimen preparation, mainly as regards powder granulometry and sample positioning, so as to minimize the error in the evaluation of the integrated signal used to estimate the crystallized volume fraction. Crystalline phases were identified by comparing the positions and relative intensities of peaks in X-ray diffraction patterns with data in the JCPDS (Joint Committee on Powder Diffraction Standards) database. Optical transmittance and absorption measurements were collected by means of a VARIAN Cary 50 spectrophotometer with a resolution of 1 nm and a PERKIN ELMER Lambda 9000 spectrophotometer with a cryostat for measurement down to 15 K with an uncertainty of ±1 K. The effects due to light reflection and scattering by the surfaces in optical absorption spectra were estimated from combined measurements of transmittance $T_{obs}$ and diffused reflectance $R_{obs}$ by means of an integrating sphere fitted to the spectrophotometer. The values of absorption coefficient $\alpha$ have been obtained by numerically solving the following system:

$$\begin{cases} T_{obs} = e^{-\alpha x}(1-R)^2 \\ R_{obs} = R(1+e^{-\alpha x}) \end{cases} \quad (1)$$

where $x$ and $R$ are the sample thickness and reflectivity, respectively. Refractive index measurements were performed using a prism coupling refractometer METRICON 2010 working at 633 nm with an uncertainty lower than $10^{-3}$. Photoluminescence (PL) and PL-excitation (PLE) patterns were obtained as contour plots of light intensity by collecting

photoluminescence spectra, with a resolution of 2 nm, at different excitation wavelengths in step of 1 nm by means of a VARIAN Eclipse spectrofluorimeter. PL decay kinetics were investigated exciting at 250 nm by means of a pulsed xenon lamp and integrating the signal in a range of 10 nm at around 460 nm, with a delay from the pulse of 10 μs and a resolution of 0.1 μs. Measurements of blue PL as a function of the temperature in the range 3–300 K were performed by means of a liquid helium cryostat and collecting through an optical fiber the light emission excited by a laser at 266 nm.

## Results and discussion

**Nanostructuring and optical transmittance.** In view of using Ga-oxide NCs as wide-band-gap light emitters in glass, the influence of NCs on the optical transmittance of the resulting material is an essential part of the basic information we need, and one of the main parameters we must control after the material production. In Ga-containing alkali-germanosilicate glasses, NCs can be generated through two successive processes we have recently found to take place in glass with a composition of $7.5Li_2O–2.5Na_2O–20Ga_2O_3–35GeO_2–35SiO_2$.[16]

For such a composition, in fact, we previously carried out small-angle-neutron-scattering measurements, which registered a well detectable maximum of the scattered intensity even before any thermal treatment, with features consistent with heterogeneities less than 10 nm in size.[16] Therefore, first, the system gives rise to nanometer sized heterogeneities uniformly dispersed in as quenched glass as a result of a liquid–liquid phase separation in the melt. Then, a secondary phase separation of the native nano-heterogeneities can be induced and controlled by means of post-synthesis thermal treatments, so as to give rise to $γ-Ga_2O_3$ NCs uniformly distributed in the glass. In Fig. 1a and b we report representative HRTEM images collected on powder of nanocrystallized material after 15 min and 2.5 h treatment at about 690 °C. This temperature corresponds to the exothermic peak in the DSC curve (Fig. S1, ESI†). TEM images and electron diffraction patterns (Fig. 1c and d) show that the nanophase consists of $γ-Ga_2O_3$ NCs with a mean diameter of 6 ± 2 nm after 15 min of treatment. Larger mean size, up to 20 nm, and more pronounced crystalline features in the diffraction pattern are observed after prolonged treatment. The comparison between X-ray diffraction patterns before and after thermal treatment shows an amount of segregated crystalline phase on the order of a few mol% after 15 min, up to the nominal content of 20 mol% of Ga-oxide after prolonged treatment of 2.5 h, as confirmed by the complete disappearance of the exothermic DSC peak (Fig. S1 and S2, ESI†). Therefore, based on the nanocrystal mean size and total amount of crystalline nanophase, the NC concentration turns out in the range $10^{17}–10^{18}$ $cm^{-3}$.

Remarkably, the $γ-Ga_2O_3$ NCs turn out to be very stable at the temperature of the thermal treatment, and we do not detect any XRD evidence of formation of the $β-Ga_2O_3$ phase even keeping the sample at 690 °C for more than 100 hours, i.e. a duration more than 40 times longer than the treatment needed to complete the nanocrystallization process. It is worth noting that

such a quite dense dispersion of NCs (up to few millions per cubic micrometer, see ESI) is compatible with negligible light scattering. The transmittance of the nano-crystallized material is indeed visually indistinguishable from the starting glass (inset of Fig. 1e). Such an outcome depends on size, concentration and refractive indexes $n_c$ and $n_g$ of nanocrystals and glass matrix, respectively, according to the expression of turbidity,[28–31]

$$\sigma_s = \frac{8\pi^3}{\lambda^4} \xi \left[ n_c (n_c - n_g) \right]^2 V_{NC}^2 \qquad (2)$$

where $\lambda$ is the wavelength, while $V_{NC}$ and $\xi$, are the NC volume and concentration, respectively. On the Ga-free sample we prepared with identical relative molar compositions of the other components – taken as a reference of the host matrix after phase separation – we measure a refractive index $n_g = 1.566 \pm 0.001$ at 632 nm. From $n_g$ and $n_c$, assuming the latter be equal to the $β-Ga_2O_3$ value of 1.93,[32] we calculate the size dependence of scattering-attenuated transmittance in Fig. 1f. It is noteworthy that $I/I_0$ can be kept above 90% (neglecting reflection losses), even at high NC concentration and Ga-oxide content, if the mean NC size is smaller than 10 nm.

**Band-to-band transitions of embedded nanocrystals.** The achievement of a nanostructured system with low scattering losses – with clear advantages for optical applications – does also allow for the first direct investigation of the $γ-Ga_2O_3$ intrinsic absorption edge, which is the second basic information we need. Although there is an adequate knowledge of the optical absorption of pure $β-Ga_2O_3$,[1,32,33] the optical properties of $γ-Ga_2O_3$ are not well known, mainly because this polymorph is a metastable phase. Particularly, no data are available on the intrinsic properties of $γ-Ga_2O_3$ NCs in glass, since the only studies on embedded variants were essentially aimed at obtaining convenient hosts for IR-emitting ions, such as $Ni^{2+}$ and $Cr^{4+}$.[15,17,34] As a result, the data in Fig. 2 constitute the first quantitative insight into the absorption edge of $γ-Ga_2O_3$ as a nanophase in a solid matrix. Fig. 2a reports the absorption coefficient $\alpha(E)$ vs. the photon energy $E$. The exponential behavior $\alpha(E) \propto \exp(E/E_U)$ is typical of the onset of band-to-band transitions in the energy region of the Urbach tail (see the inset in Fig. 2a), where $E_U$ is the Urbach energy which is related to the energy distribution of localized states at the edges of the energy gap.[35] Fig. 2a also shows the spectrum of a Ga-free reference sample. No relevant absorption contribution is observed up to energy above 5 eV, so confirming that the absorption edge in the other samples can be fully ascribed to the formation of the $γ-Ga_2O_3$ nanophase. However, the value of the optical gap energy is not directly accessible from the reported data, which does not comprises the Tauc region,[36] in which the absorption coefficient is too large to be measured in bulk samples. Looking at the inset of Fig. 2a and the temperature dependence of the iso-absorption in Fig. 2b (i.e. the spectral energy at an arbitrary fixed $\alpha$ value of 50 $cm^{-1}$), the bandgap energy at room temperature is expected at around 4.5–4.6 eV. Confirmation will be given in the next section from the analysis of the exciton peak in the luminescence excitation spectrum. The T-dependence of slope and spectral shift of the Urbach tail gives further
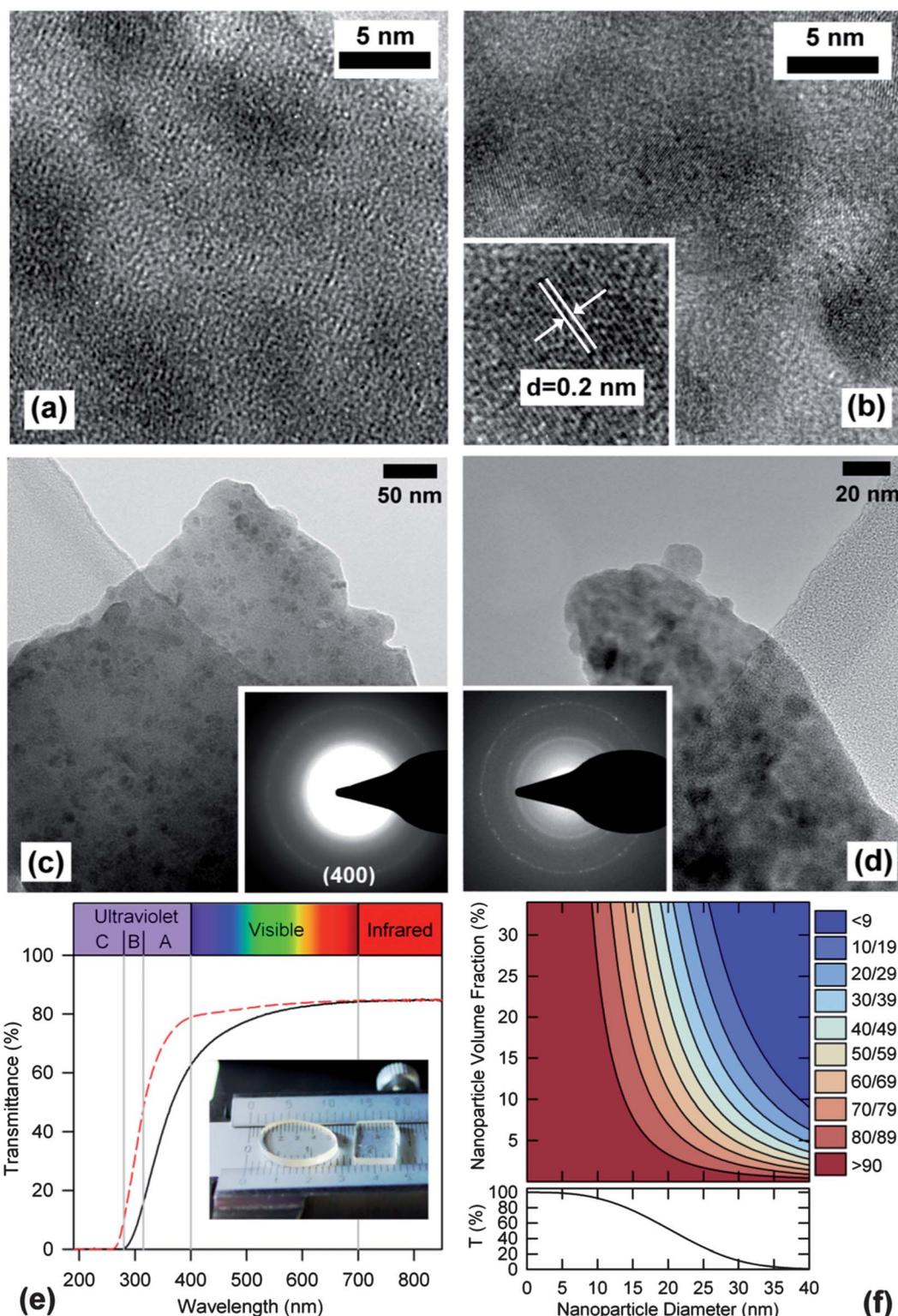
Fig. 1 TEM analysis and optical transmittance of nanostructured glass with a composition of $7.5Li_2O-2.5Na_2O-20Ga_2O_3-35GeO_2-35SiO_2$ with embedded $\gamma$-$Ga_2O_3$ NCs. (a) HRTEM image after thermal treatment of nanocrystallization at 690 °C for 15 min. (b) HRTEM image after prolonged thermal treatment of 2.5 hours. Inset: high-resolution image showing the (400) interplanar crystal spacing of $\gamma$-$Ga_2O_3$. (c) TEM image after 15 min treatment (inset: electron diffraction pattern). (d) TEM image after 2.5 h treatment (inset: electron diffraction pattern). (e) Optical transmittance of a 1.5 mm thick nanostructured glass before (dashed line) and after (full line) nanocrystallization. Inset: the image of as-quenched (left) and thermal treated (right) samples. (f) Calculated transmittance at 633 nm, accounting for scattering losses only (according to eqn (2)), as a function of nanoparticle diameter and volume fraction.
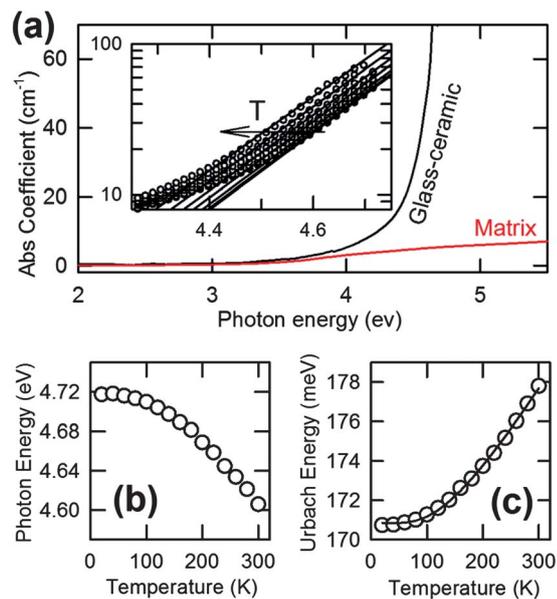
Fig. 2 Optical absorption edge of $\gamma$-$Ga_2O_3$ NCs in glass. (a) Absorption coefficient of nanostructured $7.5Li_2O$–$2.5Na_2O$–$20Ga_2O_3$–$35GeO_2$–$35SiO_2$ with embedded $\gamma$-$Ga_2O_3$ nanocrystals (glass ceramic), compared with reference Ga-free glass with the same composition of the other components (matrix). Inset: absorption coefficient in log-scale of the nanostructured glass at different temperatures in steps of about 50 K from 10 K to 300 K (lines are linear fit). (b) Temperature dependence of the energy of iso-absorption, calculated as the photon energy corresponding to fixed absorption coefficient (arbitrary chosen at 50 $cm^{-1}$). (c) Temperature dependence of the Urbach energy from the slope of the linear fit of data in (a). The line is the fit according to eqn (3).

information about the nanophase. Fig. 2c shows $E_U(T)$ data from the fit of the exponential absorption edge at different temperatures. The data permit isolation of the $T$-dependent contribution of edge broadening (due to phonon-related deviations from crystalline order) from $T$-independent contributions arising from static disorder:[35,36]

$$E_U(T) = \frac{h\nu}{\sigma} \cot h\left(\frac{h\nu}{2kT}\right) + \frac{h\nu X}{2\sigma} \qquad (3)$$

where $h\nu$ (36 ± 2 meV from the fit) is the characteristic phonon energy in the Einstein model representation of the phonon spectrum, $\sigma$ is a dimensionless parameter of the order of unity, and $X$ (31 ± 1 from the fit) is a parameter quantifying the $T$-independent contribution. The obtained $h\nu$ value, corresponding to 290 $cm^{-1}$, lies in the region of the low-energy collective phonon modes of $\gamma$-$Ga_2O_3$,[37] consistent with the assignment of the absorption edge to the intrinsic $\gamma$-$Ga_2O_3$ bandgap. The value of the $X$ parameter describes the static structural disorder and it is proportional to the mean-square deviation of the distribution of the relative atomic positions (normalized by the zero point uncertainty).[35] Interestingly, the calculated $X$ value is much larger than usually found in crystals (e.g. $X = 10^{-4}$ in quartz), and also in excess with respect to topologically disordered amorphous oxides with almost perfect short range order like pure silica, in which $X$ is about

0.2–0.3.[36,38] Larger values are only found in systems with defective short range order, lowered by coordination defects and/or network modifier ions, as in hydrogenated Si, fluorinated silica, Si-doped AsGa, and Cu-doped CdS ($X = 2–8$, 2–3, 17, and 8, respectively).[35,36,38–41] The occurrence of such a high $X$ value in $\gamma$-$Ga_2O_3$ NCs strongly points out the role of the interphase, which is likely responsible for a large amount of localized states caused by coordination mismatch and stoichiometry deviation. In fact, it is quite reasonable that band-to-band transitions are strongly influenced by interphase properties, since the surface-to-volume ratio is very large. Taking a mean NC size of 6 nm, the fraction of Ga sites at the interface is estimated about 29% of the total.

**Photoluminescence of embedded nanocrystals.** Excitation at photon energy higher than the onset of the UV absorption tail in Fig. 2 gives rise to an intense and broad visible PL in the nanostructured material. The results of the investigation of the light-emission and excitation pattern are summarized in Fig. 3a. The contour plot shows the spectral distribution of PL intensity as a function of the excitation energy. The PL pattern comprises three main contributions: in the UV, blue, and green regions (see circles in Fig. 3a). In Fig. 3b, emission and excitation spectra are extracted at representative wavelengths in the 3D pattern. As regards the UV emission, the spectral position at about 360 nm matches with the PL observed in Ga-oxide single phases and attributed to exciton-like transitions.[10,11]

This emission shows a peculiar exciton-like structure in the excitation spectrum, peaked at 275 nm, just in the spectral region of the absorption edge. The corresponding energy $E_{ex}$ (about 4.5 eV) can be used to obtain an estimation of the bandgap energy $E_G$, which should be higher than the exciton energy $E_{ex}$ just for the exciton binding energy $E_b$. Since $E_b$ in semiconductors (including wide-bandgap semiconductors) is in the range $10^{-2}$ to $10^{-1}$ eV,[42] we can consider 4.5 eV as a good estimation of $E_G$ in the present case, taking also into account that a major uncertainty is caused by the spectral width of the exciton peak (0.3 eV of full width at half maximum). The reported $E_G$ values in $Ga_2O_3$ phases, mainly from measurements of the optical absorption edge of thin films, lie in the range from 4.2 to 5.1 eV.[43–51] Such a spread of values is related to the variability of oxygen stoichiometry in Ga-oxides, the larger the oxygen deficiency, the smaller the effective bandgap.[32] Additional spread of $E_G$ values can be expected in NCs, in principle, from quantum confinement (QC). However, such an effect was rarely registered, if any, in the optical absorption spectrum of $Ga_2O_3$.[5,20] Actually, in nanosystems, the optical absorption edge arises from additive contributions of all NCs, each characterized by specific size-dependent QC according to[52]

$$\alpha(E) = \int \nu(R)\alpha_0(E - \Delta E(R))dR \qquad (4)$$

where $\alpha_0(E)$ is the expected $Ga_2O_3$ spectrum without QC, and $\Delta E(R)$ is the energy shift caused by QC in the variety of NCs of radius comprised between $R$ and $R + dR$ with distribution $\nu(R)$. As a consequence, the resulting absorption edge is strongly biased by NCs with the lowest $E_G$ (largest size and negligible QC
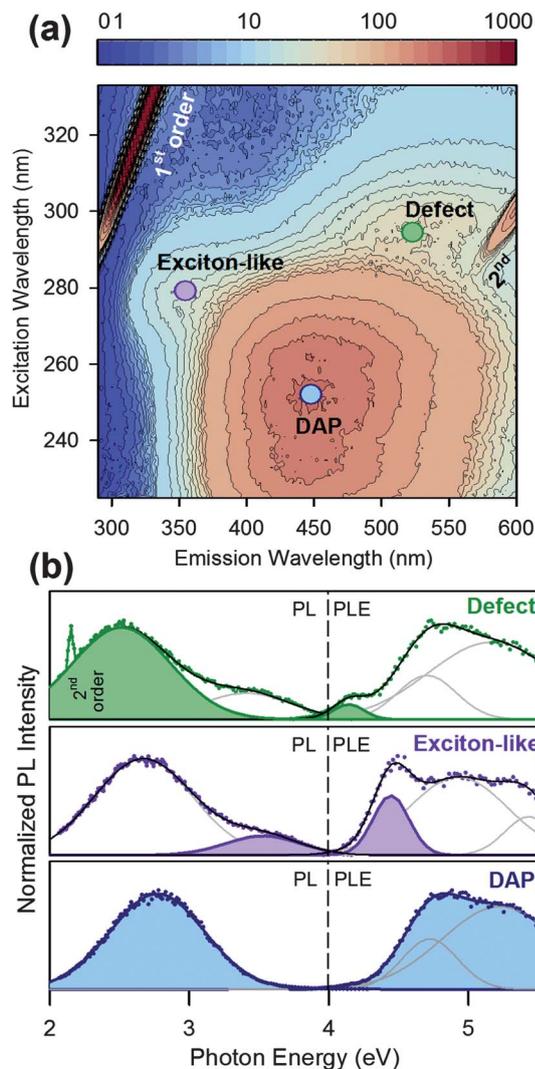
**Fig. 3** Spectral analysis of light emission and excitation of nano-structured 7.5Li$_2$O−2.5Na$_2$O−20Ga$_2$O$_3$−35GeO$_2$−35SiO$_2$ with embedded γ-Ga$_2$O$_3$ NCs. (a) Contour plot of PL intensity as a function of emission and excitation wavelength. Circles indicate the excitation (emission) wavelength of the emission (excitation) spectra in (b) according to the labels. The intense features linearly dependent on the wavelength in the upper part of the contour plot are due to the excitation light at the first and second order. (b) Right (left) hand part of the axis above (below) 4 eV: spectral distribution of light emission as a function of the exciting (emitted) photon energy at the emission (excitation) wavelength indicated in (a) by circles with the corresponding label.

effects), whose absorption contribution dominates at low energy and hides the absorption onset of smaller NCs at higher energy. Moreover, no effect is expected on $E_U$ from the convolution of exponential tails with different QC effects, since they simply shift the onset without changing the slope. For this reason, QC and stoichiometry-related shift (affecting $\Delta E$ and $\alpha_0(E)$, respectively) are hard to be disentangled in the optical absorption edge of nanosized Ga$_2$O$_3$, even taking advantage of data on the NC size distribution. Interestingly, the bandwidth of the exciton peak in the excitation spectrum permits a more

reliable analysis of consistency between the QC-related distribution of $E_{ex}$ and NC size dispersion. Broad peaks are in fact peculiar to excitons in NCs, in which the size dispersion is a relevant source of inhomogeneous broadening caused by the spread of size-dependent exciton energies. The $E_{ex}$ shift $\Delta E_{ex}$ from $E_G$ can be estimated from

$$\Delta E_{ex} = \frac{\hbar^2}{2\mu}\frac{\pi^2}{R^2} - \frac{1.8e^2}{4\pi\varepsilon_0\varepsilon_r R} \tag{5}$$

where $\varepsilon_r$ is the relative dielectric function of the nanophase at low frequency (10.2 in Ga-oxides) and $\mu$ is the reduced exciton mass, which can be substituted by the electron effective mass $m_e^*$ (0.27–0.34 $m_e$ in α- and β-Ga$_2$O$_3$ phases) neglecting the kinetic energy of the hole in the approximation $m_e^* \ll m_h^*$.[1,53] According to eqn (5), taking $m_e^* = 0.3m_e$, the data on the size distribution from TEM analysis ($\langle R \rangle = 3$ nm and $\sigma(R) = 2$ nm) give an expected broadening of the exciton peak of 0.2 eV, in semi-quantitative agreement with the experimental bandwidth of the 275 nm peak. The same evaluation provides us with an estimation of the mean value of QC shift $\Delta E_{ex}$ of approximately 0.06 eV, hard to be detected as a convoluted shift of the absorption edge, as correctly argued in a previous work.[20] This value permits however estimation of an expected $E_G$ in bulk of about 4.4 eV, important to gives us a first insight into a crucial feature of γ-Ga$_2$O$_3$ NCs grown on glass. In fact, the relatively small $E_G$ value of the related bulk phase suggests a quite relevant content of oxygen vacancies $V_O^{\cdot}$ per NC. This result is essential for the understanding of the PL properties, which drastically depend on the occurrence of $V_O^{\cdot}$ sites, especially the main blue contribution. The main component of the light-emission pattern in Fig. 3 – centered at 460 nm and extended in a broad range of the visible region – matches in fact the spectral features of the dominant luminescence observed in all light-emitting Ga-oxide materials and attributed to radiative $V_O^{\cdot}$ related to DAP recombination of band-to-band excitations.[10–14]

Consistently with this attribution, the blue PLE profile in Fig. 3b ranges from the absorption tail (at about 280 nm) to the high energy limit of the present experiment (at the onset of the vacuum UV region), as expected from band-to-band excited radiative recombination. As regards the minor green component at 530 nm, the assignment to transitions at the localized defect sites is supported by the excitation-emission pattern in Fig. 3, showing a quite restricted excitation region at around 295 nm and a large Stokes shift of the emission.

The scheme of excitation and radiative decay processes, summarized in Fig. 4a, is qualitatively consistent with previously detailed studies on stable single-phase β-Ga$_2$O$_3$ systems and doped variants.[10–14] Quantitatively, all values are updated on the basis of the present results on embedded γ-Ga$_2$O$_3$ NCs. The main light emission centered at around 460 nm is connected to the occurrence of $V_O^{\cdot}$ sites which can trap electrons from the conduction band. Subsequent transfer to excited states of complexes of oxygen and gallium vacancies $(V_O, V_{Ga})'$, behaving as acceptor sites, gives rise to radiative decay with emission of photons in the blue region.[10] Light emission may however be hindered by thermally promoted donor and acceptor ionization, which turns out to be competitive to DAP
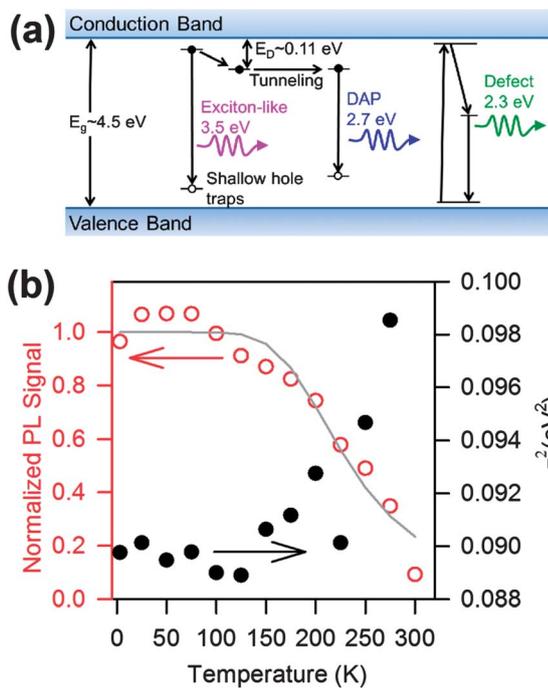
**Fig. 4** Energy levels and temperature dependence of PL. (a) Scheme of the energy levels and electronic transitions involved in the three main contributions of light emission (according to Fig. 3) in nano-structured 7.5Li$_2$O–2.5Na$_2$O–20Ga$_2$O$_3$–35GeO$_2$–35SiO$_2$ with γ-Ga$_2$O$_3$ NCs. (b) Temperature dependence, from 300 K down to 4 K, of the integrated intensity (left axis) and the second moment (right axis) of the Gaussian component describing the blue PL by exciting at 266 nm. The line is the result of the fit according to eqn (6).

recombination and can lower the integrated PL intensity $I(T)$ according to

$$I(T) \propto \frac{1}{1 + A\mathrm{e}^{-E_{d,a}/kT}} \quad (6)$$

where $E_{d,a}$ is the ionization energy of donors or acceptors, respectively. Actually, donor and acceptor ionization is expected to occurs at different temperatures: $E_{d,a}$ values of 0.05 eV and 0.45 eV were in fact found in single phase Ga-oxide (β-phase) for donors and acceptors, respectively.[10] In Fig. 4b we report the temperature dependence, from 300 K down to 3 K, of the integrated PL intensity throughout the blue component together with the bandwidth value. The data, analyzed through eqn (6), are qualitatively consistent with the results previously found in β-Ga$_2$O$_3$, but suggests that donor sites are deeper in the bandgap than in β-Ga$_2$O$_3$, with $E_d$ = 0.11 eV. The present data do not permit an estimation of acceptor ionization energy, which is however larger than $E_d$.[10] Interestingly, the PL bandwidth turns out to be only slightly temperature dependent, with a relative change of 10% at most (Fig. 4b). This fact potentially suggests a large inhomogeneous contribution caused by a variety of donor and acceptor configurations possibly related to the reduced crystalline domain and interface perturbation. However, strong electron–phonon coupling can similarly cause an almost $T$-independent homogeneous broadening. Comparison between the bandwidth of blue luminescence in the

β-Ga$_2$O$_3$ single crystal and amorphous QD colloids supported the main role of homogeneous broadening.[10,19] In our case, some insight into the role of electron–phonon coupling or defectiveness comes from the analysis of the $T$-dependence of the luminescence bandwidth $2\sigma$, according to

$$\sigma^2(T) = \sigma_{\mathrm{hom}}{}^2 + \sigma_{\mathrm{inh}}{}^2 = S\left(\hbar\omega_{\mathrm{ph}}\right)^2 \cot h\left(\frac{\hbar\omega_{\mathrm{ph}}}{2k_{\mathrm{B}}T}\right) + \sigma_{\mathrm{inh}}{}^2 \quad (7)$$

where $k_{\mathrm{B}}$ is the Boltzmann constant, $\hbar\omega_{\mathrm{ph}}$ is the mean energy of the local phonon mode coupled with the electronic transition, $S$ is the Huang–Rhys coupling constant of vibrational modes in Einstein's oscillator model, and $\sigma_{\mathrm{inh}}$ is the temperature independent contribution of inhomogeneous broadening.[54] The comparison between the low temperature experimental $\sigma$-value and the low-$T$ limit $\sigma^2(0) = S(\hbar\omega_{\mathrm{ph}})^2 + \sigma_{\mathrm{inh}}{}^2$ of eqn (7) gives information on $\sigma_{\mathrm{inh}}{}^2$ and $\hbar\omega_{\mathrm{ph}}$. The coupling parameter $S$ is in fact determined by the spectral Stokes shift $\Delta E$ between emission and excitation energies through the relationship $\Delta E = E_{\mathrm{exc}} - E_{\mathrm{emi}} = 2S\hbar\omega_{\mathrm{ph}}$, where $E_{\mathrm{emi}} = 2.7$ eV is the emission peak energy and $E_{\mathrm{exc}}$ is the excitation energy. The $E_{\mathrm{exc}}$ value cannot be directly measured, because the PL is not excited through an intra-center process, but can be estimated from the spectral position of the excitation band maximum at about 4.9 eV, after subtracting donor and acceptor ionization energies $E_d = 0.11$ eV (eqn (6) and Fig. 4b) and $E_a = 0.45$ eV (single crystal data,[10] likely an underestimation in the present case). Finally one obtains $S\hbar\omega_{\mathrm{ph}} = 0.8$ eV. Substituting this value in eqn (7), an upper limit of $\sigma_{\mathrm{hom}}(T = 0)$ may be evaluated taking the largest phonon energy compatible with the phonon spectrum of Ga-oxide, in the range 650–800 cm$^{-1}$.[37,55] Interestingly, the high energy part of the phonon spectrum contains highly localized modes restricted within the octahedral coordination shell of Ga ions.[55] Therefore, the attribution of a prevalent contribution of the blue PL bandwidth to homogeneous broadening strongly calls for electron–phonon coupling in localized defect states, decoupled from the lattice, as the acceptor sites. Nevertheless, in the present case, $\sigma_{\mathrm{hom}}{}^2(T = 0)$ turns out to be 0.74 eV$^2$ at most, to be compared with the experimental $\sigma$-value of 0.9 eV$^2$. The discrepancy suggests that in Ga-oxide NCs there is a minor but non-negligible inhomogeneous contribution of about 20% to the DAP PL broadening, probably related to the reduced crystal domain. This fact is a benefit for applications, since the spectral range turns out to be extended with limited dependence on the temperature.

**DAP balance and light emission kinetics.** The analysis of the PL decay kinetics shows an intriguing result, registering a nearly pure hyperbolic $t^{-2}$ time-dependence, typical of bimolecular recombination (Fig. 5a). Such a result is expected in the $t \to \infty$ limit for a balanced donor–acceptor system,[56] hard to be encountered in Ga oxide phases, even in pure single crystal.

At variance with a balanced system, the most common situation of excess of donors or acceptors gives instead rise to a complex kinetics, which is not exactly exponential nor hyperbolic.[10] The kinetics turns out to be complex basically because the probability for a donor electron to recombine with an acceptor hole can be strongly influenced by the competitive
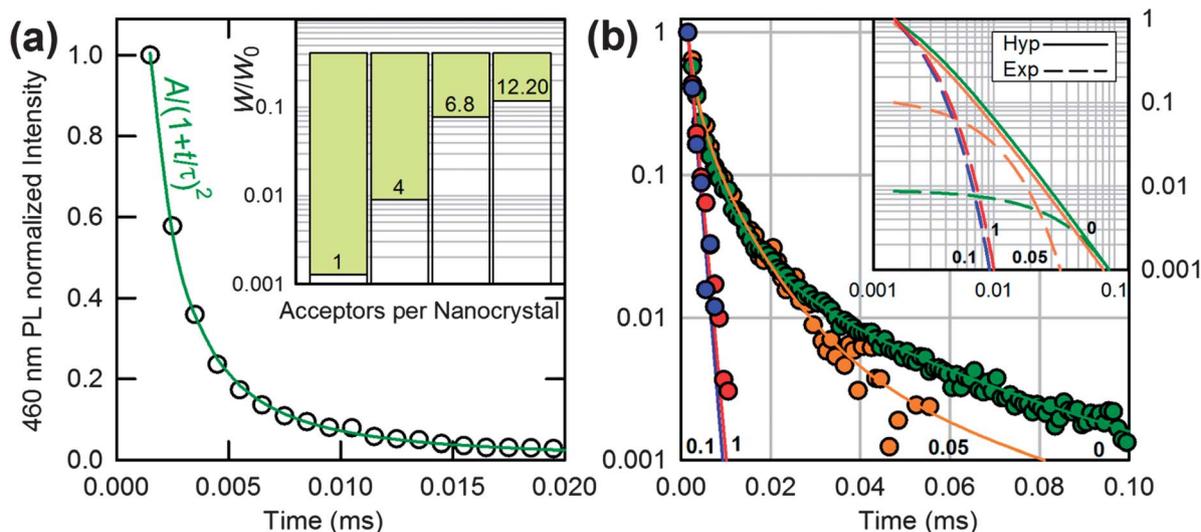
**Fig. 5** Time decay of blue PL and dependence on the acceptor number. (a) Time decay of PL at 460 nm in nanostructured 7.5Li$_2$O–2.5Na$_2$O–20Ga$_2$O$_3$–35GeO$_2$–35SiO$_2$ with embedded γ-Ga$_2$O$_3$ NCs. The line is the result of the fit of experimental point with the indicated function. Inset: the calculated range of values of recombination probability $W(r)$ (normalized to the maximum value $W_0(a)$) according to eqn (8) for different numbers of acceptors per NC (indicated in the bars), with acceptors at the vertexes of regular polyhedra inscribed in the NC. (b) Time decay in log-scale of blue PL of the undoped sample compared with samples doped with 0.05, 0.1, and 1 mol% NiO (according to labels). Lines are the result of the fit as a sum of two contributions with hyperbolic and exponential kinetics. Inset: hyperbolic and exponential contributions used to fit the data.

recombination of other donor electrons during the decay.[56] The recombination probability can in fact be written as

$$W(r) = W_0 e^{-2r/R_D} \qquad (8)$$

which is a decreasing function of the ratio between the donor–acceptor distance $r$ and the donor Bohr radius $R_D$ (1.8 nm in β-Ga$_2$O$_3$).[10] This ratio determines the overlapping of the donor electron wavefunction at the acceptor site.[56] Therefore, $W(r)$ can be sensibly modified during the decay by the progressive decrease of available acceptors at short distance from donor electrons, since the smallest DAPs undergo recombination in the first steps of the decay. Such a situation is the origin of the complex decay kinetics of blue PL in β-Ga$_2$O$_3$ single crystals.[10] In that case, an excess of donors can easily give rise to a large distribution of donor–acceptor distances with elapsing time, lacking in principle any spatial restriction to DAP recombination. Similar complex decays have however been recently observed in nanosystems as well, in condition of large deviation from compensation. Precisely, non-hyperbolic decay was observed in colloidal γ-Ga$_2$O$_3$ NCs, and analyzed as the result of a distribution of independent kinetics, each confined within a single NC.[25] Non-hyperbolic kinetics was successfully modeled in that case by the occurrence of only one acceptor per NC and several donors, all distributed on the NC surface. According to that model, a distribution of $W(r)$ arises from a sufficiently wide distribution of $r/R_D$ values within the single NC. As a consequence, the NC population gives rise to different decay contributions statistically distributed during the decay. The response turns out to be described similar to the bulk, except for the

upper limit to $r/R_D$, which in NC colloids is constrained by the NC size and the type of internal distribution of acceptors and donors (in the volume or on the surface).[25] Therefore, the hyperbolic decay we instead observe in embedded γ-Ga$_2$O$_3$ NCs represents a quite unexpected response, which deviates from bulk single crystals and colloidal γ-Ga$_2$O$_3$ NCs.

The origin of the peculiar response may be clarified looking at the effects of the reduced NC size when the conditions of crystal defectiveness deviate from the extreme situation of only one acceptor per NC. The increase of the number of acceptor sites within the limited volume of a single NC can in fact cause a drastic decrease of the range of $r/R_D$ values, with a consequent significant narrowing of the spread of $W(r)$ values given by eqn (8). As a result, when the number $N_A$ of acceptors per NC is large enough, all excited NCs are expected to have a donor electron with a nearby acceptor site almost at the shortest possible distance. This situation asymptotically approaches a bimolecular process because, in all NCs, donor electrons would have approximately the same probability of tunneling and recombination in acceptor sites. To evaluate semi-quantitatively the number of acceptors needed to have appreciable effects, we report in the inset of Fig. 5a the range of normalized recombination probability $W(r)/W_0$ in few representative cases with $1 < N_A < 20$ at a fixed NC radius (3 nm) and donor Bohr radius (1.8 nm). The range $\Delta(W(r)/W_0)$ is estimated as the spread from the maximum value $W(r_{min})/W_0$ calculated for $r_{min}$ corresponding to one lattice parameter ($a \sim 0.8$ nm in γ-Ga$_2$O$_3$) down to the minimum value $W(r_{max})/W_0$ calculated at $r_{max}$ equal to the largest donor–acceptor distance within the NC. Supposing donors and acceptors localized on the NC interphase, as

previously considered,[25] $r_{max}$ can be easily guessed in representative cases of regular distributions of $N_A$ acceptors at the vertexes of perfect polyhedra inscribed inside the NC spherical surface. In that case, $r_{max}$ can be calculated as the maximum distance between a generic point on the surface and the nearest acceptor site. Remarkably, while $\Delta(W(r)/W_0)$ ranges over almost three orders of magnitude with one acceptor per NC (giving rise to non-hyperbolic kinetics), the possible $W(r)/W_0$ values are instead squeezed in less than one order of magnitude when $N_A$ is 6 or more. As a result, only minor effects of time dependence of the recombination rate are expected, at least until only one donor electron per NC is excited (low intensity regime). In other words, the hyperbolic kinetics in our samples highlights a strictly nanostructure-dependent decay mechanism, which results in a sort of NC-confined bimolecular recombination. The process does not modify the average donor–acceptor distance for other excited electrons (belonging to different NC), and no relevant distribution of recombination probability can occur since the DAP size is comparable with $R_D$.

An insight into the expected ratio of donor-to-acceptor concentration can be obtained noticing that the single hyperbolic $1/(1 + t/\tau)^2$ dependence – over two decades – points to a spread $\Delta\tau \sim W(r_{max})^{-1} - W(r_{max})^{-1}$ significantly smaller than the mean decay lifetime itself. This fact calls for $W(r_{min})$ very close to $W(r_{max})$ with $W(r_{min}) < 3W(r_{max})$. Fixing the minimum DAP distance at $r_{min} = R_D = 2.25a$ (a realistic value, since acceptors are quite large complexes), we find $W(r_{min})/W_0 = 0.09$. In this case, $3W(r_{max})/W_0$ overcomes $W(r_{min})/W_0$ by more than a factor 2 or 3 only for $N_A$ greater than 6–8 or 12–20, respectively (Fig. 5). Remarkably, $N_A$ turns out to be comparable to $N_D$ estimated in $\gamma$-$Ga_2O_3$ colloidal NCs with a similar size ($N_D = 30$–40).[25] Bearing in mind that Ga oxide is a native donor-rich compound, our result suggests a possible role of the oxide matrix in stabilizing acceptors at the NC surface during nanocrystallization. In fact, at variance with solution-based synthesis of nanopowders, NC growth in glass involves the formation of an interphase between different oxide structures (amorphous and crystalline) with cations in quite different coordination units (mainly tetrahedral and octahedral, respectively). This structural mismatch can be the source of the gallium vacancies responsible for the formation of acceptor sites.

**Blue-to-UV tuning of luminescence by acceptor removal.** The peculiar condition of NC-confined decay kinetics of the blue PL in embedded $\gamma$-$Ga_2O_3$ NCs – with the expected strong dependence on $N_A$ – finds confirmation in data obtained on samples with Ni-doped $\gamma$-$Ga_2O_3$ NCs. Doping the investigated glass with $Ni^{2+}$ ions gives rise, in fact, to full incorporation of $Ni^{2+}$ into $\gamma$-$Ga_2O_3$ NCs upon nanocrystallization, as we found in a previous work by registering the changes of $Ni^{2+}$ crystal field absorption and IR luminescence.[15] The selective doping of NCs with $Ni^{2+}$ ions gives a tool for lowering $N_A$ by means of heterovalent cations with oxidation state smaller than $Ga^{3+}$. Bearing in mind that acceptors consist of $(V_O, V_{Ga})'$ complexes – and that the presence of native $V_{Ga}$ is somewhat related to the oxygen deficiency determined by the synthesis conditions – we expect that $Ni^{2+}$ ions could lower the number of $Ga^{3+}$ vacancies required by charge neutrality at a fixed oxygen defectiveness. As

a matter of fact, there are relevant effects of $Ni^{2+}$ doping on the PL of $\gamma$-$Ga_2O_3$ NCs: changes are registered in lifetime, intensity, and spectral distribution of PL. These effects ultimately suggest the real possibility of tuning the nanophase light emission from a dominant blue DAP-PL of an undoped system to UV emission in the case of $Ni^{2+}$ doped NCs. The main effects on PL kinetics are summarized in Fig. 5b, reporting the decay curves of blue PL in samples with different levels of $Ni^{2+}$ doping. Deviation from pure hyperbolic decay is observed at the lowest doping level (0.05 mol%), whereas an exponential decay prevails at heavier doping. The decay curves are reproduced by a sum $aI_{Hyp} + (1 - a)I_{Exp}$ of two contributions (fitting curves in Fig. 5b and components in the inset). The first term $aI_{Hyp}$ accounts for emitted light from excited NCs decaying through DAP recombination – following a hyperbolic function $I_{Hyp} = 1/(1 + t/\tau)^2$ – whereas $(1 - a)I_{Exp}$ describes the contribution of NCs in which there are additional efficient decay channels giving rise to a resulting kinetics with an exponential term $I_{Exp} = \exp(-t/\tau)$. The latter decay paths are likely related to donor electrons recombining with holes in traps distinct from acceptor sites – or directly in the valence band in NCs fully depleted of Ga vacancies and, consequently, with no acceptor sites. The lifetime of DAP recombination turns out to be of the order of μs, with less than 10% of difference between undoped and 0.05 mol% $Ni^{2+}$ doped samples (1.4 and 1.3 μs, respectively), whereas the lifetime of the exponential contribution shows a shortening of more than one order of magnitude from undoped to heavily $Ni^{2+}$ doped samples (40 and 1.1 μs, respectively). This result points to a key role of excitation migration among donor sites toward the sites of competitive decay, according to the behavior expected for a diffusion-limited relaxation.[57,58] Such a relevant increase of diffusion-limited relaxation suggests that the $N_A$ lowering is accompanied by the increase of $N_D$ at increasing Ni doping. As a result, $Ni^{2+}$ ions not only decrease $N_A$, but also enhance the probability of non-radiative processes. The comparison between PL patterns of Ni doped samples in Fig. 6, and the pattern of an undoped sample in Fig. 3 (all collected in identical conditions of excitation and detection geometry) shows that the overall PL emission (not only the DAP related blue PL) is lowered in the doped material. This fact suggests that $Ni^{2+}$ ions act also as quenchers of the host PL, as often observed in transition metal doped matrices. Interestingly, Ni-doping does not only enhance non-radiative decay channels, but also UV PL. This fact suggests the formation of shallow hole traps which promote radiative recombination of donor electrons in the final levels at energy closer to the valence band than acceptor levels. The patterns in Fig. 6 in fact register the increase of a UV band centered at 350 nm at increasing Ni doping. Specifically, this band becomes evident after the drastic lowering of the blue PL, particularly when the Ni content changes from 0.05 to 0.1 mol% and the kinetics changes from hyperbolic to exponential.

In this regard, it is noteworthy the intriguing coincidence between the number of $Ni^{2+}$ ions per NC (about 5 and 10 $Ni^{2+}$ ions per NC, for 0.05 mol% and 0.1 mol% of NiO, respectively) and the expected minimum number of 6–8 acceptors per NC needed to keep the $W(r)$ distribution significantly narrower than
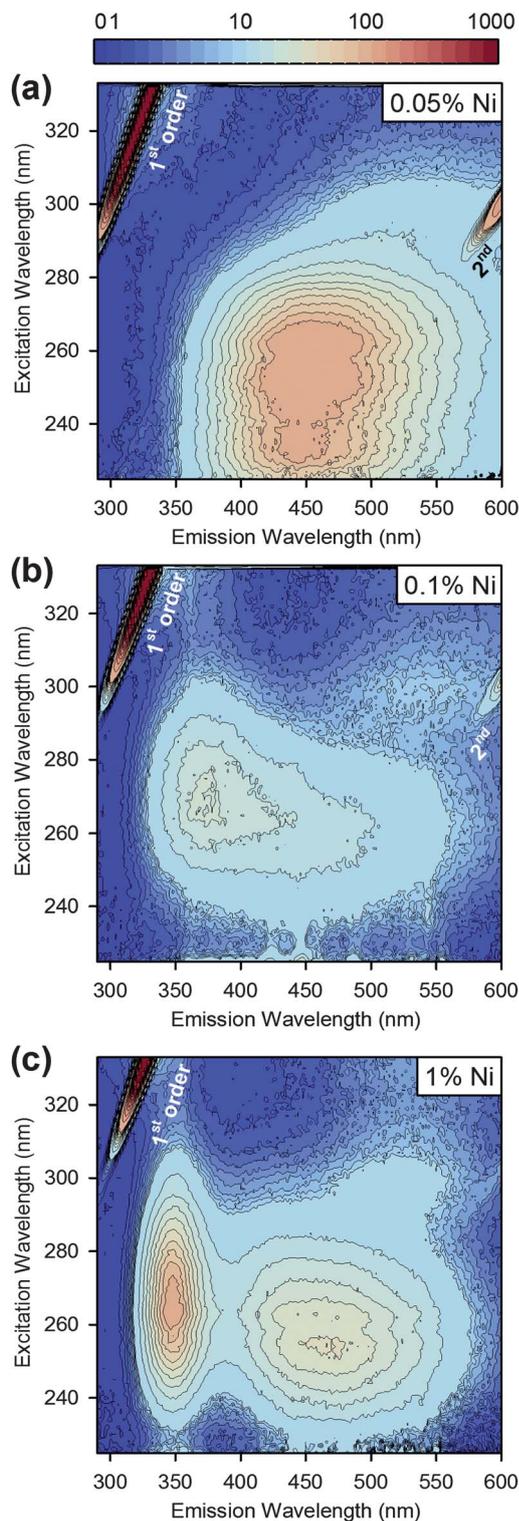
Fig. 6 Light emission and excitation of NiO doped variants of nanostructured glass. Contour plots of PL intensity as a function of emission and excitation wavelengths in samples with (a) 0.05 mol%, (b) 0.1mol%, (c) 1 mol% NiO.

in the non-hyperbolic kinetics described by the one-acceptor model (inset of Fig. 5a). In other words, Ni$^{2+}$ ions seem to prevent the formation of Ga vacancies and, when the concentration of NiO overcomes the quantity compatible with the

native oxygen deficiency, the NiO excess introduces additional $V_O$ sites and defects. Therefore, the results in Fig. 5 and 6 definitely assess the feasibility of controlling donor–acceptor compensation and disproportion in embedded NCs, taking advantage of the ratio between NC size and $R_D$, and the doping with heterovalent ions.

## UV-to-visible conversion

We finally present a first demonstration of one of the most immediate breakthroughs deriving from the implementation of γ-Ga$_2$O$_3$ NCs in the glass matrix. In Fig. 7 we report the proof of concept of a solar-blind UV-to-visible passive converter. The 'solar-blind' region is identified in Fig. 7a by the spectral range in which the solar spectral irradiance at the Earth surface vanishes. As a matter of fact, the comparison with transmittance and excitation spectra in Fig. 7b shows that the nanostructured material turns out to be transparent and
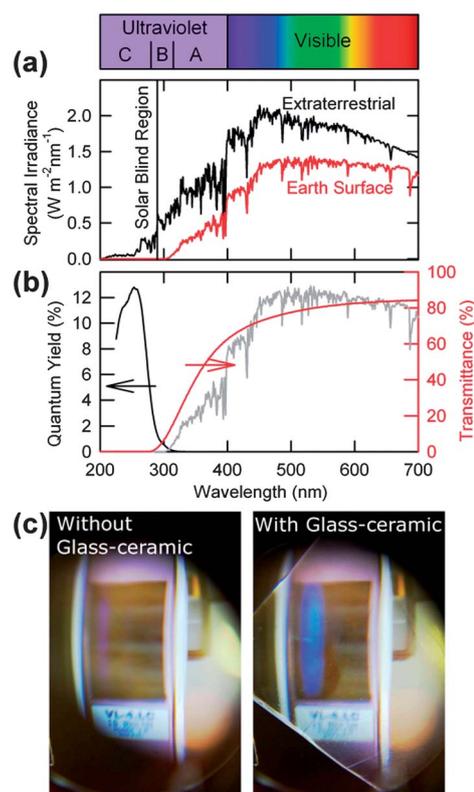


Fig. 7 UV-to-visible conversion. (a) Representative data of the mean spectral irradiance of solar radiation above the atmosphere and at the Earth surface, with indication of the conventional identification of the UV-C solar blind spectral regions. (b) Value of the quantum yield of blue luminescence as a function of the excitation wavelength in nanostructured 7.5Li$_2$O−2.5Na$_2$O−20Ga$_2$O$_3$−35GeO$_2$−35SiO$_2$ with embedded γ-Ga$_2$O$_3$ nanocrystals, compared with the optical transmittance of a 1.5 mm thick sample and the solar spectral irradiance at the Earth surface. (c) Images of a mercury lamp optimized for the emission at 254 nm collected by a commercial photocamera without (left) and with (right) a plate of the nanostructured material in the focal plane of a simple optics consisting of two lenses placed in front of the camera lens. In the image on the left it is possible to observe the weak violet contribution of the lamp emission.

inactive (not light-emitting) when exposed to the visible and near UV part of the solar spectrum, since the whole excitation spectrum of the embedded NCs is restricted to the solar-blind UV-C region. Importantly, from a quantitative point of view, the efficiency of the excitation of blue PL is about 10% (internal quantum yield). As a result, in a 1.5 mm thick sample, almost all photons at 250 nm are absorbed (Fig. 1e), and the external UV-to-blue conversion yield is more than 10%. The resulting material looks like a transparent window for optics, with no fluorescence under exposure to visible and near UV light. By contrast, under UV-C illumination under daylight conditions, the fluorescence is visible and bright (Fig. 7, and Fig. S3, ESI†). Fig. 7c shows how the material works as a UV-C sensitive fluorescent transparent window and acts as an UV-to-visible converter. When it is placed in the focal plane of an optics in front of a commercial camera (Fig. S4, ESI†) collecting the image of a Hg lamp at 254 nm, it provides a bright blue image of the UV-C source superimposed to the day-light scene.

## Conclusions

Two types of results have been obtained in the present work. On the one hand, we have demonstrated the feasibility of innovative nanostructured systems consisting of easily workable glass-based optical materials with UV-C excited light emission from a Ga-oxide crystalline phase introduced as NCs. This result – and the related one concerning the doping induced spectral tailoring of the PL from blue to UV – appears strictly connected to potential applicative breakthrough. On the other hand, the most seminal result regards the overall knowledge gained on the photophysics of $\gamma$-Ga$_2$O$_3$ NCs in a glass matrix. The detailed and quantitative analysis of the optical absorption spectrum, the excitation and light emission pattern, the $T$-dependence of PL intensity and bandwidth, and the PL decay kinetics, all together permit us to make previously lacking data available, and us to indicate the direction for obtaining optimized variants of the present system.

Importantly, a novel and unexplored effect of spatial confinement on the DAP recombination process has been highlighted when the nanocrystal size becomes comparable with the donor Bohr radius and not too a low number of acceptors occur in the single nanocrystal. This gives an unprecedented rationale to design analogue systems with other compositions.

## Acknowledgements

## Notes and references

1 H. He, R. Orlando, M. A. Blanco, R. Pandey, E. Amzallag, I. Baraille and M. Rérat, *Phys. Rev. B: Condens. Matter Mater. Phys.*, 2006, **74**, 195123.

2 E. G. Víllora, K. Shimamura, Y. Yoshikawa, Y. Ujiie and K. Aoki, *Appl. Phys. Lett.*, 2008, **92**, 202120.

3 L. Nagaraja, R. A. De Souza, D. Samuelis, I. Valov, A. Börger, J. Janek, K.-D. Becker, P. C. Schmidt and M. Martin, *Nat. Mater.*, 2008, **7**, 391.

4 S. C. Vanithakumari and K. Kar Nanda, *Adv. Mater.*, 2009, **21**, 3581.

5 T. Chen and K. Tang, *Appl. Phys. Lett.*, 2007, **90**, 053104.

6 L. C. Tien, C. H. Ho, X. T. Yao and J. R. Cai, *Appl. Phys. A*, 2011, **102**, 105.

7 J. Díaz, I. López, E. Nogales, B. Méndez and J. Piqueras, *J. Nanopart. Res.*, 2011, **13**, 1833.

8 Y. Li, T. Tokizono, M. Liao, M. Zhong, Y. Koide, I. Yamada and J.-J. Delaunay, *Adv. Funct. Mater.*, 2010, **20**, 3972.

9 G. Chen, F. Abou-Galala, Z. Xu and B. M. Sadler, *Opt. Express*, 2008, **16**, 15060.

10 L. Binet and D. Gourier, *J. Phys. Chem. Solids*, 1998, **59**, 1241.

11 K. Shimamura, E. G. Víllora, T. Ujiie and K. Aoki, *Appl. Phys. Lett.*, 2008, **92**, 201914.

12 T. Harwig, F. Kellendonk and S. Slappendel, *J. Phys. Chem. Solids*, 1978, **39**, 675.

13 G. Blasse and A. Bril, *J. Phys. Chem. Solids*, 1970, **31**, 707.

14 Z. i Liu, X. Jing and L. Wang, *J. Electrochem. Soc.*, 2007, **154**, H440.

15 V. N. Sigaev, N. V. Golubev, E. S. Ignat'eva, V. I. Savinkov, M. Campione, R. Lorenzi, F. Meinardi and A. Paleari, *Nanotechnology*, 2012, **23**, 015708.

16 V. N. Sigaev, N. V. Golubev, E. S. Ignat'eva, B. Champagnon, D. Vouagner, E. Nardou, R. Lorenzi and A. Paleari, *Nanoscale*, 2013, **5**, 299.

17 S. V. Lotarev, A. S. Lipatiev, N. V. Golubev, E. S. Ignat'eva, G. E. Malashkevich, A. V. Mudryi, Yu. S. Priseko, R. Lorenzi, A. Paleari and V. N. Sigaev, *Opt. Lett.*, 2013, **38**, 492.

18 C.-C. Huang and C.-S. Yeh, *New J. Chem.*, 2010, **34**, 103.

19 T. Wang and P. V. Radovanovic, *Chem. Commun.*, 2011, **47**, 7161.

20 T. Wang, S. S. Farvid, M. Abulikemu and P. V. Radovanovic, *J. Am. Chem. Soc.*, 2010, **132**, 9250.

21 S. S. Farvid, T. Wang and P. V. Radovanovic, *J. Am. Chem. Soc.*, 2011, **133**, 6711.

22 S. I. Maximenko, L. Mazeina, Y. N. Picard, J. A. Freitas Jr, V. M. Bermudez and S. M. Prokes, *Nano Lett.*, 2009, **9**, 3245.

23 N. Pinna, G. Garnweitner, M. Antonietti and M. Niederberger, *J. Am. Chem. Soc.*, 2005, **127**, 5608.

24 C. Otero Areán, A. López Bellan, M. Peñarroya Mentruit, M. Rodríguez Delgado and G. Turnes Palomino, *Microporous Mesoporous Mater.*, 2000, **40**, 35.

25 M. Hedge, T. Wang, Z. L. Miskovic and P. V. Radovanovic, *Appl. Phys. Lett.*, 2012, **100**, 141903.

26 J. Wang, Y. Yoo, C. Gao, I. Takeuchi, X. Sun, H. Chang, X.-D. Xiang and P. G. Schultz, *Science*, 1998, **279**, 1712.

27 S. Brovelli, N. Chiodini, R. Lorenzi, A. Lauria, M. Romagnoli and A. Paleari, *Nat. Commun.*, 2012, **3**, 690.

28 C. F. Bohren and D. Huffman, *Absorption and scattering of light by small particles*, John Wiley, New York, 1983.

29 W. Caseri, *Chem. Eng. Commun.*, 2009, **196**, 549.

30 R. Lorenzi, A. Lauria, N. Mochenova, N. Chiodini and A. Paleari, *J. Non-Cryst. Solids*, 2011, **357**, 1888.

31 S. Zhou, N. Jiang, B. Wu, J. Hao and J. Qiu, *Adv. Funct. Mater.*, 2009, **19**, 2081.

32 M. F. Al-Kuhaili, S. M. A. Durrani and E. E. Khawaja, *Appl. Phys. Lett.*, 2003, **83**, 4533.

33 Y. Zhang, J. Yan, G. Zhao and W. Xie, *Phys. B*, 2010, **405**, 3899.

34 B. Wu, S. Zhou, J. Ren, Y. Qiao, D. Chen, C. Zhu and J. Qiu, *J. Phys. Chem. Solids*, 2008, **69**, 891.

35 G. D. Cody, T. Tiedje, B. Abeles, B. Brooks and Y. Goldstein, *Phys. Rev. Lett.*, 1981, **47**, 1480.

36 K. Saito and A. J. Ikushima, *Phys. Rev. B: Condens. Matter Mater. Phys.*, 2000, **62**, 8584.

37 Y. Hou, L. Wu, X. Wang, Z. Ding, Z. Li and X. Fu, *J. Catal.*, 2007, **250**, 12.

38 A. Paleari, F. Meinardi, S. Brovelli, A. Lauria, R. Lorenzi and N. Chiodini, *Appl. Phys. Lett.*, 2007, **91**, 141913.

39 R. Lorenzi, S. Brovelli, F. Meinardi, A. Lauria, N. Chiodini and A. Paleari, *J. Non-Cryst. Solids*, 2011, **357**, 1838.

40 S. R. Johnson and T. Tiedje, *J. Appl. Phys.*, 1995, **78**, 5609.

41 M. Grus and A. Sikorska, *Phys. B*, 1999, **266**, 139.

42 M. Dvorak, S.-H. Wie and Z. Wu, *Phys. Rev. Lett.*, 2013, **110**, 016402.

43 J. Hao and M. Cocivera, *J. Phys. D: Appl. Phys.*, 2002, **35**, 433.

44 M. Rebien, W. Henrion, M. Hong, J. P. Mannaerts and M. Fleischer, *Appl. Phys. Lett.*, 2002, **81**, 250.

45 M. Passlack, E. F. Schubert, W. S. Hobson, M. Hong, N. Moriya, S. N. G. Chu, K. Konstadinidis, J. P. Mannaerts, M. L. Schnoes and G. J. Zydzik, *J. Appl. Phys.*, 1995, **77**, 686.

46 M. Orita, H. Ohta, M. Hirano and H. Hosono, *Appl. Phys. Lett.*, 2000, **77**, 4166.

47 H.-G. Kim and W.-T. Kim, *J. Appl. Phys.*, 1987, **62**, 2000.

48 P. Wu, Y.-M. Gao, R. Kershaw, K. Dwight and A. Wold, *Mater. Res. Bull.*, 1990, **25**, 357.

49 A. Ortiz, J. C. Alonso, E. Andrade and C. Urbiola, *J. Electrochem. Soc.*, 2001, **148**, F26.

50 N. Ueda, H. Hosono, R. Waseda and H. Kawazoe, *Appl. Phys. Lett.*, 1997, **70**, 3561.

51 H. H. Tippins, *Phys. Rev. A*, 1965, **140**, 316.

52 S. Brovelli, A. Baraldi, R. Capelletti, N. Chiodini, A. Lauria, M. Mazzera, A. Monguzzi and A. Paleari, *Nanotechnology*, 2006, **17**, 4031.

53 M. Passlack, E. F. Schubert, W. S. Hobson, M. Hong, N. Moriya, S. N. G. Chu, K. Konstadinidis, J. P. Mannaerts, M. L. Schnoes and G. J. Zydzik, *J. Appl. Phys.*, 1995, 77, 686.

54 M. Leone, S. Agnello, R. Boscaino, M. Cannas and F. M. Gelardi, in *Silicon-Based Materials and Devices*, ed. H. S. Nalwa, Academic, New York, 2001, vol. 2, p. 1.

55 D. Dohy, G. Lucazeau and A. Revcolevschi, *J. Solid State Chem.*, 1982, **45**, 180.

56 D. G. Thomas, J. J. Hopfield and W. M. Augustyniak, *Phys. Rev.*, 1965, **140**, A202.

57 M. J. Weber, Luminescence, *Phys. Rev. B: Condens. Matter Mater. Phys.*, 1971, **4**, 2932.

58 S. Brovelli, N. Chiodini, F. Meinardi, A. Monguzzi, A. Lauria, R. Lorenzi, B. Vodopivec, M. C. Mozzati and A. Paleari, *Phys. Rev. B: Condens. Matter Mater. Phys.*, 2009, **79**, 153108.